Fuel cell systems for transportation: Status and trends

Rajesh K. Ahluwalia *, Xiaohua. Wang

Argonne National Laboratory, Argonne, IL 60439, USA

Abstract

The U.S. program for the development of direct hydrogen-fueled automotive fuel cell systems has established ambitious performance and cost targets for the 2010 and 2015 time frames. These targets include peak and rated power efficiencies of 60% and 50%, respectively, specific power and power densities of $650\,\mathrm{We\,kg^{-1}}$ and $650\,\mathrm{We\,L^{-1}}$, and manufactured costs of \$45 and $30\,\mathrm{kWe^{-1}}$ for $80\,\mathrm{kWe^{-1}}$ net systems in the 2010 and 2015 systems, respectively. In this paper, we discuss the use of fuel cell system models to examine the performance and projected manufactured costs of 2005 systems and the improvements needed to meet the 2010 and 2015 system level targets. It appears possible to meet most of the 2010 performance targets with advances such as the nano-structured thin film electrocatalysts and a modified electrolyte membrane capable of operating at up to 95 °C, at least for short periods. To meet the 2015 targets, however, the fuel cell systems may need to operate without pressurization at higher temperatures of up to 120 °C without the need to humidify the fuel gas and air, along with several other improvements in stack and balance-of-plant components. Our simulations provide quantitative estimates of the various performance and cost parameters of the near-term and the advanced systems that can achieve the targets set for automotive fuel cell system development.
Published by Elsevier B.V.

Keywords: Fuel cell systems; Polymer electrolyte membrane; Heat rejection; Water management; Air management; Transportation

1. Introduction

Fuel cells offer many advantages over the internal combustion engines (ICE) for vehicular applications because they are energy efficient, clean, and fuel flexible. Hydrogen fuel cell systems have the potential to reach 60% peak efficiency on lower heating value (LHV) basis. On-board the vehicle, conversion of hydrogen to traction power produces water only. Hydrogen can be produced from a variety of sources including fossil fuels such as natural gas, renewables such as solar and wind power, biomass, and nuclear energy.

Cost and durability are generally regarded as the major challenges to commercialization of fuel cells. Size, weight, and system simplicity are also important to the adoption of fuel cells in light duty vehicles. Fuel cell systems (FCS) must be reduced in cost before they can be competitive with internal combustion engines. The cost of automotive ICEs is currently about \$25–35 kW^{-1}; a fuel cell system needs to cost less than \$50 kW^{-1} for the technology to be competitive [1]. Adequate

durability of fuel cell systems under rapidly varying driving conditions has not been established; they need to be as durable and reliable as current internal combustion engines, i.e., 5000 h lifespan (150,000 miles equivalent) and able to function over the full range of ambient conditions (−40 to +40 °C).

Air management for fuel cell systems is a challenge because today's compressor technologies are not ideally suitable for automotive fuel cell applications. In addition, thermal and water management for fuel cells are issues that are not yet fully resolved. Fuel cell operation at lower temperatures creates a small difference between the operating and ambient temperatures, necessitating large heat exchangers [1]. Fuel and air feed streams need to be humidified in a highly controlled manner for proper operation of fuel cells. Whereas having to carry consumable water on-board the vehicle is considered unacceptable, recovering water formed in the fuel cell for humidifying the inlet gases adds to the complexity of the system.

Finally, the size and weight of current fuel cell systems must be further reduced to meet the stringent requirements for automobiles. Size and weight reduction applies not only to the fuel cell stack (catalysts, membranes, gas diffusion media, and bipolar plates) but also to the ancillary components making up the balance of plant [1].

* Corresponding author. Tel.: +1 630 252 5979; fax: +1 630 252 5287.
  E-mail address: walia@ne.anl.gov (R.K. Ahluwalia).

Table 1
DOE/Freedom CAR technical targets

Direct hydrogen fuel cell power system		Target		
Characteristic	Units	2005	2010	2015
System cost	$ kWe^{-1}	125	45	30
System efficiency @ 25% rated power	%	60	60	60
System efficiency @ rated power	%	50	50	50
System power density, specific power	W L^{-1}, kg^{-1}	500	650	650
Stack cost	$ kWe^{-1}	65	25	15
Stack efficiency @ 25% rated power	%	65	65	65
Stack efficiency @ rated power	%	55	55	55
Stack power density, specific power	W L^{-1}, kg^{-1}	1500	2000	2000
MEA cost	$ kWe^{-1}	50	10	5
MEA performance @ rated power	mW cm^{-2}	600	1000	1000
MEA degradation over lifetime	%	10	10	5
PGM cost	$ kWe^{-1}	40	5	3
PGM content (peak)	g kWe^{-1}	2.7	0.5	0.4
PGM loading (both electrodes)	mg cm^{-2}	0.7	0.3	0.2
Membrane cost	$ m^{-2}	200	20	20
Bipolar plate cost	$ kWe^{-1}		5	3
CEM system cost	$	600	400	200

In this paper, we discuss the status of current fuel cell system technology relative to the DOE/FreedomCAR targets listed in Table 1. The focus of this paper is on identifying the gaps in current technology, and the likely future advancements in technology that may overcome the shortfalls, to enable meeting the listed targets.

2. Near-term fuel cell systems (Argonne 2005 FCS)

Fig. 1 is a schematic of an 80 kWe pressurized FCS configuration (Argonne 2005 FCS) considered as being an idealized representation of the 2005–2006 technology [2]. The polymer electrolyte fuel cell (PEFC) stack in Fig. 1 operates at 2.5 atm
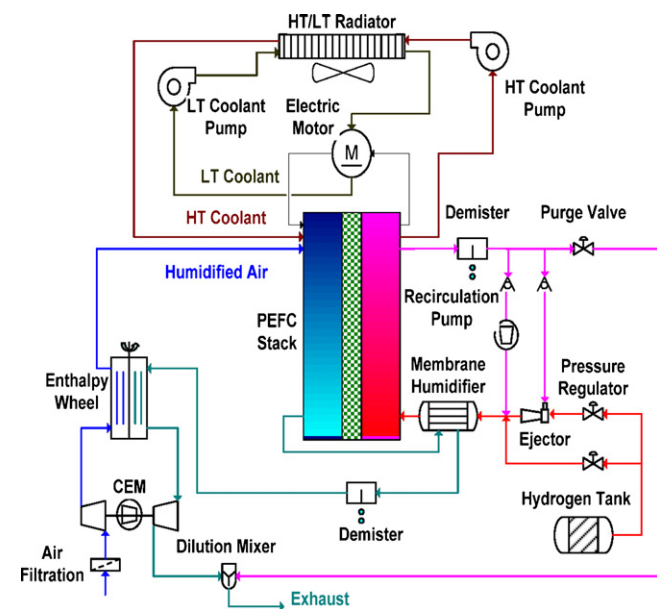

Fig. 1. Argonne 2005 FCS schematic diagram. Argonne 2010 FCS shares the same schematic but with improved materials and appropriately modified operating conditions.

at rated power, 80 °C cell temperature, 50% O$_2$ utilization and 70% per-pass H$_2$ utilization. The cell MEA consists of anode and cathode catalyst inks deposited onto the gas diffusion layers (GDL), which are hot-press laminated with the 50 μm-thick Nafion membrane. The Pt loading is 0.50 mg cm^{-2} on the cathode and 0.25 mg cm^{-2} on the anode. The flow channels are fabricated from 2 mm-thick expanded graphite plates, with each plate having cooling channels. The air management subsystem consists of a compressor–expander module (CEM) with a liquid-cooled motor, mixed axial and radial flow compressor, variable-nozzle radial inflow turbine, and airfoil bearings. The fuel management subsystem includes a hybrid ejector-hydrogen pump to recirculate a portion of the spent anode gas. The water management subsystem uses an enthalpy wheel humidifier (EWH) for the cathode feed and a membrane humidifier (MH) for the anode feed. At rated power, the feed gases are humidified to 60% relative humidity (at the stack temperature). The system is designed to be water balanced, i.e., only the water produced in the stack is used for humidifying the feed gases. The dual-loop heat rejection subsystem has a high-temperature circuit for supplying coolant at 70 °C to the stack, and a low-temperature circuit for supplying coolant at 55 °C to the vehicle traction motor and the CEM motor. The coolant in both circuits is aqueous ethylene glycol solution. The following are some major conclusions from a detailed analysis of the steady state and dynamic performance of the FCS shown in Fig. 1.

- Meeting the target of 50% system efficiency at rated power requires the stack to operate at 0.7 V cell^{-1} or higher, and results in stack specific power and power density being lower than the targets of 1500 W kg^{-1} and 1500 W L^{-1}.
- The near-term targets for stack specific power, power density and precious-metal loading (1 g Pt kW^{-1}) can be satisfied, but only by relaxing the system efficiency target.
- Durabilities of the Pt electrocatalyst finely dispersed on high-specific area carbon support and of the perfluorosulfonic acid
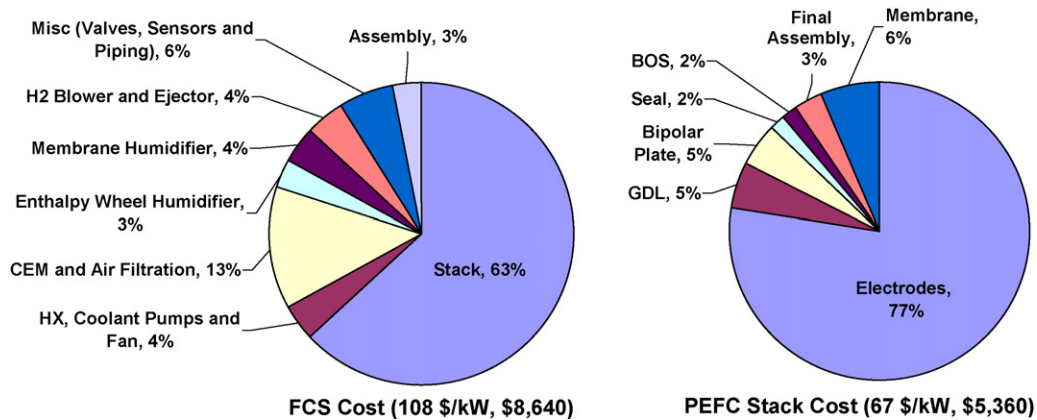
Fig. 2. Projected cost of the Argonne 2005 FCS and components [3].

(PFSA) membrane remain important unresolved issues. One reason for the high Pt group metal (PGM) loading is the requirement that the performance targets need to be met at the end of life.

- In a pressurized fuel cell system, it is important to include an expander to recover some of the pressure energy in the spent cathode air. The overall efficiency at rated power suffers without an expander in the air management subsystem and the Pt loading is correspondingly higher (per net kW of power produced).
- Heat rejection from a PEFC stack operating at 80 °C is problematic; it is even more difficult in a system without an expander. Compared to an ICE, the radiator in the FCS requires ~60% larger frontal area and four-to-five times as much fan power to provide the necessary cooling for all anticipated driving conditions and ambient temperatures.

Fig. 2 presents the projected cost breakdown for the FCS with 0.65 V cell voltage at rated power (600 mW cm^{-2} power density, 45% system efficiency). At 50,000 units/year volume production, the projected manufactured cost is about 108 $ kW^{-1}, with the PEFC stack as the largest contributor (63%) to the overall cost, followed by the air management subsystem (13%) and the water management subsystem (7%) [3]. The electrodes in the MEA account for 77% of the stack cost; much of the cost of the electrodes is due to the high Pt content and the price of Pt.

3. Intermediate-term fuel cell systems (Argonne 2010 FCS)

It is clear from the results shown in Fig. 2 that the Pt loading must be greatly reduced in order to meet the intermediate- and long-term cost targets for automotive fuel cell systems. Our analytical model indicates that the key to reducing the Pt load-

Table 2
Alternative system configurations and components to meet future targets

	Argonne 2005 FCS	Argonne 2010 FCS	Argonne 2015 FCS
Stack subsystem			
Membrane	PFSA: 50 μm	Modified PFSA: 30 μm	High T membrane
Electrocatalyst	Pt C^{-1}, 0.75 mg cm^{-2} Pt total loading	Pt Alloy, 0.3 mg cm^{-2} Pt total loading	Pt alloy or non PM
GDL	275 μm Non-woven carbon	Non-woven carbon + micro porous layer	Non-woven carbon + micro porous layer
Bipolar plate	2 mm expanded graphite	Graphite/metal	Graphite/metal
Cell power density	666 mW cm^{-2} at 0.65 V	740 mW cm^{-2} at 0.68 V	TBD
Temperature	80 °C	>90 °C	≤120 °C
Air management subsystem			
Pressure	Pressurized—2.5 atm	Pressurized—2.5 atm	Ambient pressure
Technology	CEM	CEM	Blower (BMM)
Water management subsystem			
Humidification	External	External/internal	None
Technology	EWH + MH	MH + MH advanced flow field	None
Thermal management subsystem			
Radiator concept	Standard automotive LT + HT circuits	Advanced automotive LT + HT circuits	Standard automotive LT + HT circuits
Stack coolant	Ethylene glycol	Ethylene glycol	Ethylene glycol
Fuel management subsystem			
Fuel H$_2$	High purity	FC quality	FC quality
Anode gas recirculation	Ejector/blower	Ejector/blower	Dead ended
Purge	Periodic	Periodic	Continuous

ing is to improve the catalyst durability, i.e., with a fresh catalyst (beginning-of-life performance) there is <10% difference in current density at 0.7 V if the Pt loading is reduced from 0.2 to 0.5 mg cm^{-2} in the cathode and from 0.1 to 0.25 mg cm^{-2} in the anode. For our 2010 configuration (see Table 2), therefore, we have chosen an alternative MEA design that is based on nano-structured thin film (NSTF) ternary-Pt catalyst supported on organic whiskers [4]. This NSTF catalyst has shown significantly enhanced stability against surface area loss from Pt dissolution when compared to conventional Pt/C dispersed catalysts under both accelerated voltage cycling from 0.6 to 1.2 V and real-time start stop cycling [4]. Also, NSTF catalyst support-whiskers have shown total resistance to corrosion when held at potentials up to 1.5 V for 3 h, conditions at which the carbon support gets severely corroded.

Recent work at DuPont [5] and 3 M [6] has led to an improved understanding of potential mechanisms that lead to membrane failure and strategies for preventing such failures. Modified PFSA membranes with chemical stabilization, mechanical reinforcement, and peroxide mitigation strategies have shown significant decreases in fluoride loss and increased lifetimes in simulated drive cycle tests [4]. It now appears feasible to operate the stacks at temperatures of 90 °C or higher, since the new modified PFSA membrane with stabilizing additives and reduced number of carboxylic end groups has shown good oxidative stability in load cycling tests at 90 °C for >4000 h [4].

Fig. 3 shows the modeled polarization curve of a stack with the NSTF catalyst and a 30 μm-thick modified PFSA membrane (equivalent weight ~850) at 90 °C. The catalyst, a ternary Pt/Co$_x$/Mn$_y$ alloy with Pt to transition metal ratio of 3:1, is supported on organic whiskers that are assumed to have 5×10^9 cm^{-2} area density, 1 μm height, and 50 nm diameter. Consistent with the experimental data, our model indicates that the relative humidity of the feed streams must be controlled to prevent flooding of the thin NSTF catalysts or membrane dryout. Fig. 4 shows the optimum cathode stoichiometry (SR) and relative humidity (RH) of the cathode air at stack inlet as a function of the current density normalized with respect to the current density at rated power (1.1 A cm^{-2} at 0.684 V and 2.5 bar). The optimum conditions at part load have been determined from the compressor operating map, water mass transfer in the enthalpy
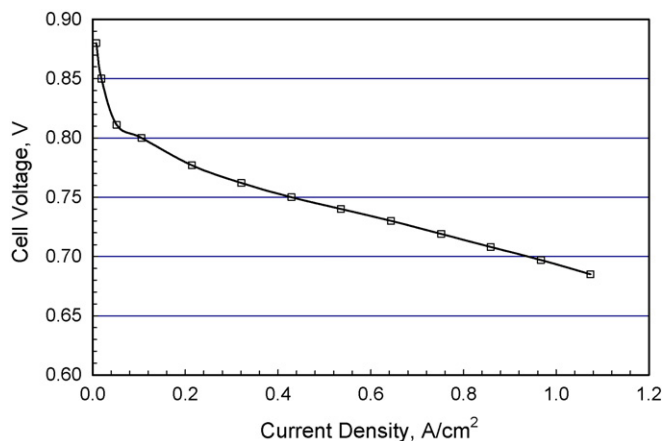

Fig. 3. Polarization curve of the pressurized stack at 90°C.

wheel humidifier and the membrane humidifier, and the stack polarization curves for different pressures, anode/cathode inlet RH, and anode/cathode SR. Fig. 4 indicates that because of the increase in cathode RH with the decrease in current density (i.e., mass flow rate), the cathode stoichiometry must be raised in order to prevent flooding of the thin catalysts at part load conditions. At the optimum operating conditions, the spent gases at the stack outlet are just saturated, although liquid water does form in the catalyst layers. The higher operating temperature (90 °C vs. 80 °C) and lower inlet RH (50% vs. 60%) imply that the stack with the NSTF catalyst runs much drier than the stack with the dispersed catalyst, and the problems of water management in the gas diffusion layers and the flow fields are considerably simplified. Under normal operating conditions, there is no liquid water in the cathode flow fields but the thin NSTF catalyst layers are prone to flooding if the inlet RH and cathode SR are not properly controlled.

Fig. 5a presents the waste heat produced in the stack as a function of the net FCS power. If this FCS is used to propel a Ford Taurus class family sedan, the maximum continuous heat load on the radiator is 53 kW at the 100 mph top vehicle speed and 51 kW at 55 mph on 6.5% grade [6]. Heat rejection is more challenging when driving on grade than at the top speed because of the smaller amount of ram air available at the lower speed. We have looked at the possibility of making the radiator more
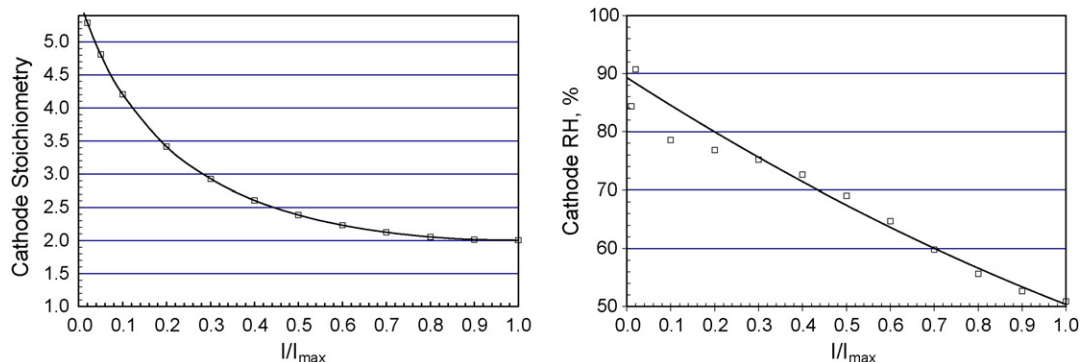

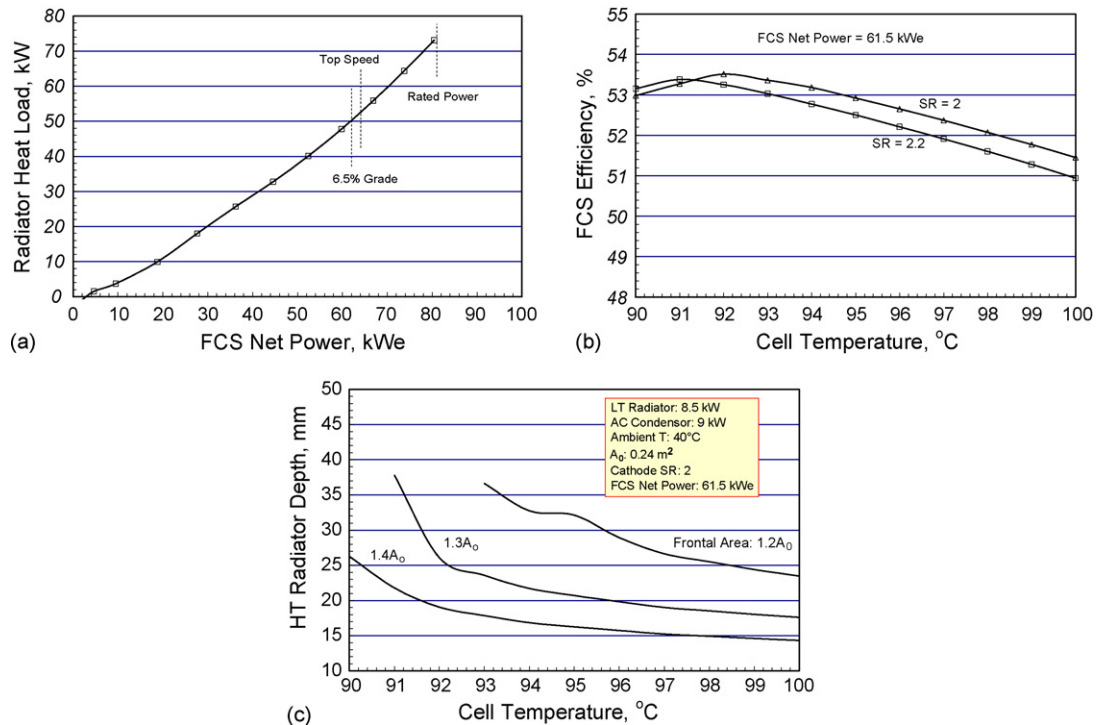Fig. 4. Stack operating conditions at constant H$_2$ utilization.

Fig. 5. Heat rejection in FCS: (a) heat load, (b) effect of cathode SR and (c) effect of cell temperature.

compact by allowing the stack temperature to rise while driving on grade. Fig. 5b indicates that the cathode stoichiometry must be reduced from the optimum value shown in Fig. 4 if the stack temperature is allowed to rise, otherwise the membrane dries out, the stack efficiency decreases, and more waste heat has to be rejected. Fig. 5c shows the effect of stack temperature on the radiator depth and frontal area needed to reject the waste heat produced while generating 61.5 kWe net FCS power at 40 °C ambient temperature. The results are for a radiator with 25-louver fins/inch and a 500 W blower that first cools the LT radiator and an A/C condenser. Fig. 5c indicates that, compared to an ICE for the same vehicle platform, a 20–30% larger frontal area is needed if the radiator depth is 25 °mm and the stack temperature is allowed to rise to 92–98 °C while driving on grade. Although the FCS radiator is considerably larger than its ICE counterpart, it is significantly more compact than the radiator needed for the 2005-FCS stack [2]. There are at least three reasons why the radiator for the FCS with the NSTF catalyst is more compact than the radiator for the stack with the dispersed Pt catalyst: the higher peak coolant temperature (87–93 °C vs. 75 °C) means that a 33–50% larger temperature difference driving force is available for rejecting heat to the ambient air at 40°C: improved catalyst durability and use of a thinner membrane (30 µm vs. 50 µm) allow the stack to operate at a higher cell voltage (684 mV vs. 650 mV) with lower Pt loading; and a smaller amount of waste heat is generated because the stack is more efficient at the higher cell voltage (54.7% vs. 51% stack efficiency at rated power). The latent heat load is negligible, whereas a significant fraction of water is formed as a liquid if the stack is operated at 80 °C. As a result of the higher cell voltage and the drier operation, the radiator heat load at 6.5% grade

is considerably smaller, 51 kW vs. ~65 kW for the 2005 FCS [2].

3.1. Stack subsystem

Fig. 6 shows a unit cell of the PEFC stack [3]. The alloy catalyst has a Pt loading of 0.2 mg cm^{-2} in the cathode and 0.1 mg cm^{-2} in the anode. The catalyst is laid down on crystalline organic whiskers as a sputter-deposited thin film to produce roll-good catalyst layers that are hot-pressed onto the membrane [7]. The anode and cathode gas-diffusion layers (GDL) are 275 µm thick non-woven carbon fibers before compression. The bipolar plates are made from expanded graphite. Each bipolar plate is made from two 1 mm-thick half plates with cooling channels on one side and a serpentine flow field on the other side. The FCS has two identical stacks, 219 cells/stack, electrically connected in series. At the rated power point, 2.5 bar compressor discharge pressure, 50% O$_2$ utilization and 70% H$_2$
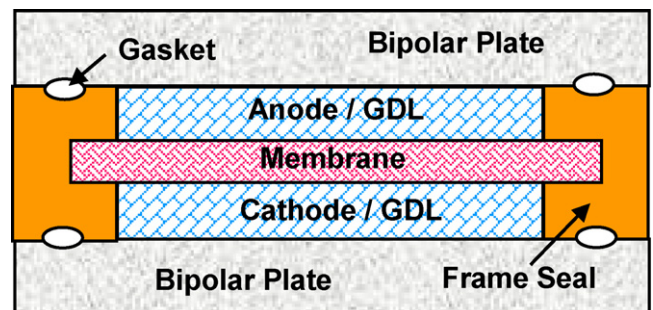

Fig. 6. Unit cell of the PEFC stack [3].

Table 3
Stack component weights/volumes

	V (L)	W (kg)
MEA total	6.6	5.6
Bipolar plate	27.7	23.1
Gaskets	0.3	0.4
Frame seal	1.9	1.2
Endplate	2.5	2.7
Current collector	0.1	2.4
Insulator	0.6	1.1
Outer wrap	1.9	3.4
Tie bolts	0.8	6.0
Stack total	42	46

utilization per pass, the stacks combine to produce 87 kWe at 300 V. Assuming that the cells can be fabricated with 85% electrochemically active area, Table 3 shows that the bipolar plates account for ∼65% of the estimated 42 L total stack volume and ∼50% of the estimated 46 kg total stack weight.

Table 4 indicates that the stack with NSTF ternary-catalyst and 30 μm membrane has the potential to meet the DOE 2010 targets of 0.5 g kWe^{-1} Pt loading and 2000 We L^{-1} stack power density, but some further weight reduction is needed to meet the specific power target of 2000 We kg^{-1}. At rated power, the calculated stack efficiency is 54.7%, just slightly below the target of 55%, because of losses due to H_2, O_2, and N_2 crossover. We calculate that ∼0.4% of H_2 feed is lost as it crosses over to the cathode, ∼0.04% of O_2 in cathode air feed crosses over to the anode and reacts with H_2, and about 0.02% of N_2 in cathode air feed crosses over to the anode. Our model includes a 1% purge of spent anode gas to limit N_2 concentration in the recycled anode gas stream to 4% at the stack inlet and 8% at the stack outlet at rated power [8]. The steady-state N_2 concentration in the recycled stream nearly doubles – 8% at stack inlet and 16% at stack outlet – at 10% power. The anode purge fraction will likely be higher than 1% if the fuel H_2 has impurities such as N_2, CO, and H_2S [9].

3.2. Air management subsystem

The Argonne 2010 FCS incorporates the air management subsystem being developed at Honeywell and is shown in Fig. 7 [10]. It consists of a mixed-flow axial compressor, radial inflow turbine and a liquid-cooled induction motor mounted on a single shaft that is supported on airfoil bearings. The maximum shaft speed is 110,000 rpm, with a minimum idling speed of

Table 4
Stack performances

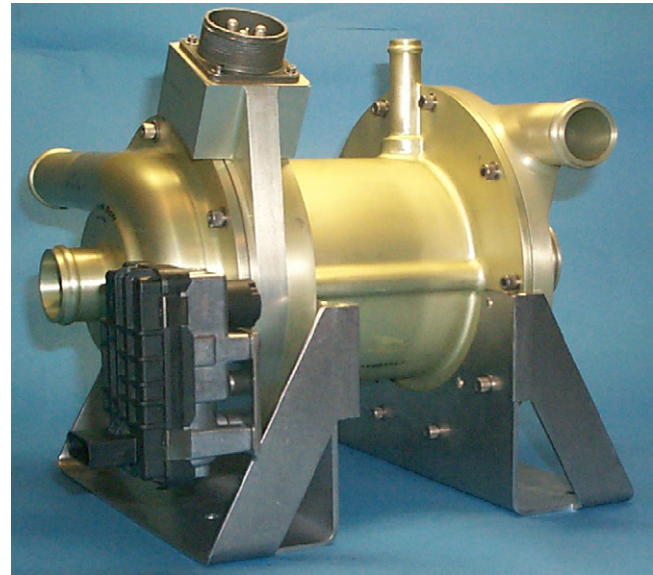| Cell V at rated power	mV	685
Stack gross power	kW	87.0
Active membrane area	m^2	11.8
Pt loading	g kW^{-2}	0.41
Current density	A cm^{-1}	1.1
Power density	mW cm^{-2}	740
Stack specific power	W kg	1900
Stack power density	W L	2070

Fig. 7. Honeywell's compressor–expander–motor module.

36,000 rpm required by the bearings. At the design flow rate, the turbo-compressor requires 11.2 kW to supply 90.4 g s^{-1} air at 2.5 bar and 78% efficiency, of which the turbine supplies 6.4 kW by expanding the spent cathode air at 80% isentropic efficiency and the balance comes from the motor. At 92% motor efficiency and 92% inverter-controller efficiency, the net DC power consumed by the motor-controller unit is 5.7 kWe.

As is typical of turbo-machines, the compressor discharge pressure, compressor efficiency, and expander efficiency all decrease at partial loads. For example, the compressor discharge pressure is only 1.7 bar at 50% flow and 1.3 bar at 25% flow. The compressor/expander efficiencies also decrease to 75/78% at 50% flow and 30/30% at 10% flow [11,12].

3.3. Fuel management subsystem

Because the fuel cell operates at less than 100% H_2 utilization per pass, the Argonne 2010 FCS includes a hybrid ejector-blower to recycle the spent anode gas. A hybrid device is needed since a single ejector of fixed geometry cannot recycle the spent H_2 over
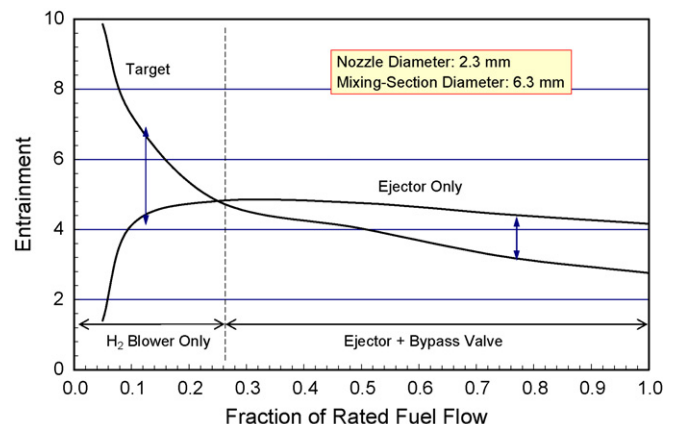

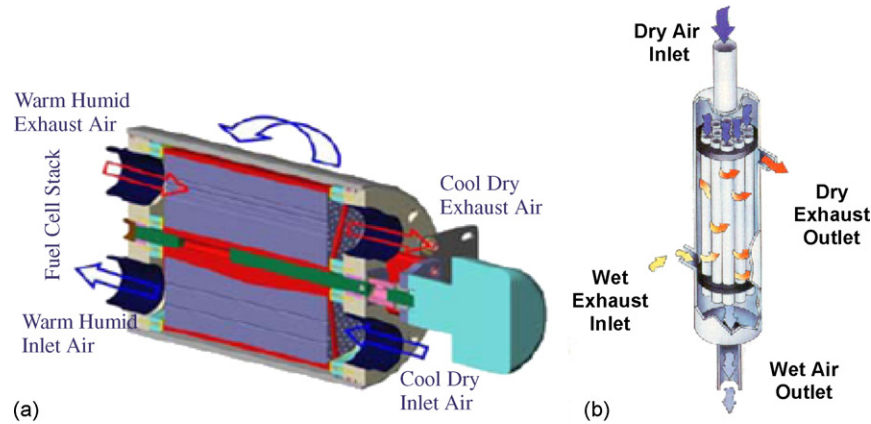Fig. 8. Performance of an ejector.

Fig. 9. Water management system components: (a) enthalpy wheel humidifier and (b) membrane humidifier.

the complete range of flow rates. For example, Fig. 8 compares the amount of spent anode gas (mixture of H_2, H_2O, and N_2) that can be entrained (g-gas/g-H_2), using fuel H_2 as the motive gas, with the amount that must be entrained (target) to maintain 70% H_2 utilization per pass. For the purpose of this calculation, the ejector orifice has been sized for rated H_2 flow rate ($1.3\,g\,s^{-1}$) at 8 bar H_2 supply pressure, the mixing section has been sized for 2 psi pressure lift, and the H_2 supply pressure is regulated down at part loads. Fig. 8 indicates that a single ejector can recycle the spent anode gas for 25–100% fuel H_2 flow rates, but a recirculation blower is needed for flow rates less than 25% of flow at rated power.

3.4. Water management subsystem

Fig. 9 shows a schematic of an enthalpy wheel humidifier (EWH) used to humidify the air discharged from the compressor by transferring moisture from the spent cathode air [13]. The EWH consists of a thin-walled, desiccant-coated 400 cpi (cells in^{-2}) monolith that is rotated (nominally at 60 rpm) to contact the dry and wet streams at different times during a single revolution. The desiccant absorbs moisture as it contacts the wet stream and releases moisture as it contacts the dry stream. At the design point, $8.2\,g\,s^{-1}$ moisture is transferred from the saturated spent cathode air at 90 °C to the dry air discharged from the compressor at 2.5 bar and, depending on the ambient temperature, at 135–160 °C. The mass transfer is accompanied with heat transfer such that the dry air is cooled to within 10 °C of the stack temperature while the spent cathode air is heated so that more power is extracted from the expander. Whereas, heat and mass transfer occur in the opposite directions at the rated power point, they are in the same direction at part load conditions at which the compressor delivers air at lower pressures and at temperatures lower than the stack temperature.

Fig. 9 also includes the schematic of a membrane humidifier (MH) used to humidify the fuel H_2 by transferring moisture from the spent cathode air [14]. The MH consists of 600 Nafion tubes that have 1 mm internal diameter, 1.2 mm external diameter, and $\sim0.3\,m^2$ membrane area. At the rated power point, the total amount of mass transfer of water vapor is about $0.7\,g\,s^{-1}$.

3.5. Heat rejection subsystem

Since the heat rejection subsystem in an FCS can be bulky, a study was conducted to evaluate alternatives to the standard automotive radiators (louver fins, 15 fins inch^{-1}). We evaluated advanced automotive (louver fins, 25 fins inch^{-1}), microchannel (plain fins, 40 fins inch^{-1}) and foam (8 w% Al alloy, 40 pores inch^{-1}) configurations by considering specific heat transfer, specific pressure drop, and fan power. In terms of the fan power for specified frontal area and heat rejection, the microchannel configuration was judged as the best performer and the foam configuration as the worst performer. Also, the advanced automotive configuration performed better than the standard automotive design. We selected the advanced configuration because of concerns with fouling of the tightly spaced fins in the microchannel configuration. Table 5 lists the requirements and operating

Table 5
Heat rejection systems

Coolant pump			
Flow rate	kg s^{-1}	3.5	$\Delta P = 20$ psi, $\Delta T = 5$ °C
Power	kWe	0.7	70% combined pump and motor efficiency
Volume	L	3	
Weight	kg	2	
Radiator Fan			
Air flow rate	kg s^{-1}	2.5	55 mph at 6.5% grade
Fan head	Pa	125	55% combined fan and motor efficiency
Fan power	kWe	0.5	
Volume	L	10	
Weight	kg	2	
Radiator			
Heat duty	kW	49	55 mph at 6.5% grade
Frontal area	m^2	0.31	Fin pitch = 985 m^{-1}
Fin area	m^2	13.2	Fin thickness = 75 μm
Depth	cm	2.5	
Volume	L	19.9	Advanced automotive design, 90/93 °C Stack T
Weight	kg	8.4	

Table 6
FCS performance and parasitic loads

Cell V at rated power	mV	685
PEFC stack	kWe	87.0
CEM motor	kWe	5.5
Enthalpy wheel motor	We	30
Radiator fan	kWe	0.5
Coolant pump	kWe	0.8
H_2 recirculation pump	We	200
FCS efficiency	%	50

Table 7
FCS specific power and power density

	W (kg)	V (L)
PEFC stack	46	42
Air management system	18	15
Fuel management system	7	9
Heat rejection system	12	36
Water management system	9	11
Miscellaneous	9	11
Total	101	124
FCS specific power (We kg^{-1})	790	
FCS power density (We L^{-1})		640

conditions for the coolant pump, radiator fan, and the radiator.

3.6. FCS performance

Table 6 lists the power produced by the PEFC stack and the parasitic loads at rated power. The cell voltage was selected for 50% net efficiency at rated power.

Fig. 10 shows the steady-state system efficiency at different loads. The FCS nearly meets the peak efficiency target of 60% but at about 15% of rated power rather than at 25% power as stated in Table 1. The peak efficiency and the location of the peak efficiency are determined largely by the maximum CEM turndown. The results in Fig. 10 are for an assumed 20:1 turndown and are for reference only. In automotive applications, it may not be possible to operate the stack continuously at rated power, the radiator fan runs intermittently, the H_2 recirculation pump is not always needed, and the CEM motor may be overloaded for short periods during acceleration or not powered during deceleration. Thus, the transient FCS efficiency can be higher or lower than the steady-state values shown in Fig. 10.

Table 7 presents the weight and volume of the various subsystems. The FCS appears capable of meeting the 2010 specific power target of 650 We kg^{-1}, but the specific power density target of 650 We L^{-1} may be difficult to meet (especially if the system definition is expanded to include other components such as the control electronics) partly because of the bulky radiator. The radiator can be made more compact if it is sized for lower ambient temperatures (e.g., 35 °C rather than 40 °C) when driving at 55 mph on 6.5% grade.
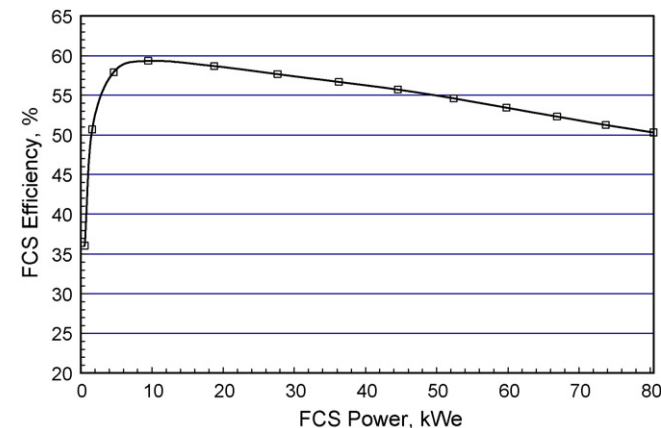
4. Far-term fuel cell system

Fig. 2 indicates that the cost of the balance-of-plant (BOP) components alone exceeds the 2010 target cost of the entire fuel cell system. The Argonne 2015 FCS configuration shown in Fig. 11 presents some conceptual possibilities for achieving further cost reductions by simplifying the BOP. The compressor–expander module can be replaced with a blower if the stack performance can be improved to the extent that pressurization is not necessary. The system can be greatly simplified if a high-temperature polymer electrolyte becomes available that does not require that the feed gases be humidified. Absent the need for a water management subsystem and the associated anode flooding issue, it may be possible to dead-end the anode channels and employ continuous purging to control the build-up of impurities. The cost of the overall system would become even more attractive if non-precious metal catalysts are developed successfully. It should be noted, however, that breakthroughs in electrolyte and non-precious metal catalyst technologies might not be critical to meeting the long-term cost targets. For example, the degradation data for the NSTF catalyst already shows the possibility of reducing the total Pt loading to 0.2 mg cm^{-2} while meeting the end-of-life performance targets.

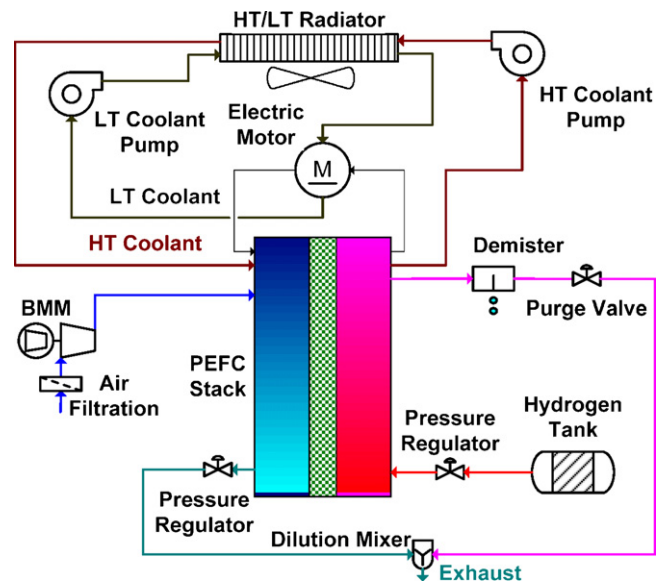Fig. 10. FCS steady-state efficiency at part load.
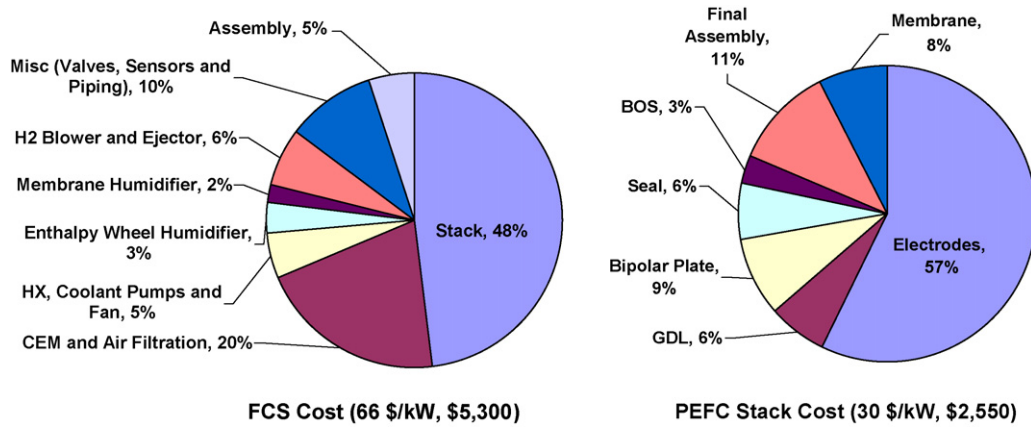

Fig. 11. Argonne 2015 FCS.

Fig. 12. Projected cost of Argonne 2010 FCS.

5. Assessment of results

Fig. 12 presents a preliminary, high-level projection of the manufactured cost of the intermediate-term Argonne 2010 FCS [15]. The projection is based on a bottom-up, activities-based costing method for the stack components; it does not include the cost of stack conditioning and the original equipment manufacturer's (OEM's) mark-ups. Fig. 12 indicates that the PEFC stack with the NSTF catalyst technology has the potential of meeting the 2010 DOE cost target of $30 kWe^{-1}. Experimental data indicate that the NSTF catalyst may satisfy the goals of <40% loss of electrochemically active surface area (ECSA) due to start/stop cycles and 40 mV voltage loss after 100 h at 1.2 V [4,5]. Experimental data also indicate that the modified PFSA membrane may satisfy the goal of 5000 h durability with load cycling; the durability under realistic driving conditions remains to be demonstrated, however.

The stack technology has reached a level of maturity that some attention can be turned to the BOP components. The data in Fig. 12 suggests that the cost of BOP components must be reduced by nearly two-thirds to meet the system cost target of $45 kWe^{-1}. The following are some ways of accomplishing this.

- A bottom-up cost study is needed to determine whether the compressor–expander–motor modules can be assembled for less than $400 at high volume manufacturing. The $1080 estimated cost for the CEM unit included in Fig. 12 results is based on consensus and extrapolation of experience with non-automotive applications. As a reference, automotive superchargers, which use essentially the same technology as the turbo compressor in the CEM unit but without the high-speed, high-power motor, reportedly cost much less than $400 at the factory.
- The anode-gas membrane humidifier (MH) is projected to cost about $110. One way of reducing the MH cost would be to enhance mass transfer by using tubes with thinner walls. As the stack membrane continue to get thinner (18 μm composite membranes are available), it may be possible to eliminate the anode-gas humidifier altogether and rely only on water transfer from the cathode to the anode.

- A bottom-up cost study may show that the centrifugal fans ($340 estimated cost of the fuel management system) can be less expensive or that the alternatives, such as vane recirculation pumps, are cheaper to build. The anode gas system may have to be simplified (e.g., by doing away with the ejector) to reduce cost at the expense of efficiency.
- The heat rejection system in the Argonne 2010 FCS is expensive ($270 estimated cost) and bulky. Alternative methods and layouts (e.g., side-by-side arrangement of HT and LT radiators) need to be considered.

Acknowledgments

Appendix A

The performance of Argonne 2005 FCS and Argonne 2010 FCS reported in this work is based on GCtool [16] models of the two systems. The important assumptions and sources used in determining the performance of the components comprising the two systems are summarized below.

The polarization curves for a stack with dispersed catalysts (Argonne 2005) were derived from the published kinetics of the hydrogen oxidation (HOR) and oxygen reduction reactions (ORR) with optimized electrode structures [17]. The transport properties of the PFSA membrane (equivalent weight = 1100) were determined from published correlations for ionic conductivity, water uptake, water diffusivity, and permeabilities of hydrogen, oxygen and nitrogen [18,19].

The polarization curves for a stack with NSTF catalysts (Argonne 2010 FCS) were derived from a model formulated using measured mass and specific activities of ternary catalysts, electrochemical surface area and experimental data for a single

cell and a 20-cell stack [4,5]. The stack model uses measured ionic conductivity for a modified (chemically stabilized, reduced number of carboxylic end groups) PFSA membrane with an average equivalent weight of 850.

The performance of the air management subsystem is based on DOE targets for compressor, expander and electric motor. There is some initial data to suggest that the targets can be met at the component level [10] but additional data is needed to demonstrate and verify the performance of a full-scale matched compressor, expander and motor set.

The performance of the anode gas subsystem is based on a model for a supersonic ejector [20] and the operating map of a commercially available hydrogen recirculation pump.

The performance of the water management subsystem is based on models for enthalpy wheel humidifier and membrane humidifier. These models have been validated against experimental data taken with subscale devices [21].

The performance of the heat rejection subsystem is derived from a model of an automotive radiator that uses published curves for heat transfer and pressure drops with plain and louver fins and metal foams.

References

[1] Hydrogen, Fuel Cells, and Infrastructure Technologies Program: Multi-Year Research, Development and Demonstration Plan, http://www1.eere.energy.gov/hydrogenandfuelcells/mypp, 2006.

[2] R. K. Ahluwalia, X. Wang, R. Kumar, Fuel Cell Systems Analysis, FY 2006 Annual Progress Report, DOE Hydrogen Program, pp. 870–874, November 2006.

[3] E. J. Carlson, P. Kopf, J. Sinha, S. Sriramulu, Y. Yang, Cost Analysis of PEM Fuel Cell Systems for Transportation, NREL/SR-560-39104, September 2005.

[4] M. K. Debe, S. J. Hamrock, R. T. Atanasoski, Advanced MEAs for Enhanced Operating Conditions, FY 2006 Annual Progress Report, DOE Hydrogen Program, pp. 692–697, November 2006.

[5] G. Escobedo, M. Gummalla, R. B. Moore, Enabling Commercial PEM Fuel Cells with Breakthrough Lifetime Improvements, FY 2006 Annual Progress Report, DOE Hydrogen Program, pp. 706–712, November 2006.

[6] R.K. Ahluwalia, X. Wang, J. Power Sources Vol.139 (2005) 152–164.

[7] M. K. Debe, J. M. Larson, W. V. Balsimo, A. J. Steinbach, R. J. Ziegler, Membrane Electrode Assemblies, United States Patent, US 6,613,106, September.2, 2003.

[8] R.K. Ahluwalia, X. Wang, Buildup of Nitrogen in Direct Hydrogen Polymer-Electrolyte Fuel Cell Stacks, J. Power Sources 17 (2007) 63–71.

[9] D. Guro, G. Keenan, Fuel Cell Grade Hydrogen Purity Requirements and the Impact on Purification, Analysis, and Cost, 2006 Fuel Cell Seminar, November 13–17, 2006.

[10] M. K. Gee, Cost and Performance Enhancements for a PEM Fuel Cell System Turbocompressor, FY 2005 Annual Progress Report, DOE Hydrogen Program, pp. 985–988, 2005.

[11] R.K. Ahluwalia, X. Wang, A. Rousseau, R. Kumar, J. Power Sources 130 (2003) 192–201.

[12] R.K. Ahluwalia, X. Wang, J. Power Sources 152 (2005) 233–244.

[13] R. A. DuBose, C. Hanson P. J. Fehl, R. Matus, Method of Species Exchange and an Apparatus Therefore, United States Patent, US 6,780,227, August 24, 2004.

[14] Perma Pure LLC, Fuel Cell Humidification Using Nafion® Moisture Exchange Devices, www.permapure.com, 2006.

[15] S. Lasher, J. Sinha, Y. Yang S. Sriramulu, Direct Hydrogen PEMFC Manufacturing Cost Estimation for Automotive Applications, 2007 DOE Hydrogen Program Review, Arlington, VA, May 15–18, 2007.

[16] H. K. Geyer R. K. Ahluwalia, GCtool for Fuel Cell Systems Design and Analysis: User Documentation, ANL-98/8, March 1998.

[17] H.A. Gasteiger, J.E. Panels, S.G. Yan, J. Power Sources 127 (2004) 162–171.

[18] T.E. Springer, T.A. Zawodzinski, S. Gottesfeld, J. Electrochem. Soc. 138 (1991) 2334–2342.

[19] C. Mittelsteadt, M.S Umbrell, Gas Permeability in Perfluorinated Sulfonic Acid Polymer Membranes, 207th Electrochemical Society Meeting, Toronto, Canada, May 15–20, 2005.

[20] R.K. Ahluwalia, H.K. Geyer, ASME J. Eng. Gas Turbines Power 118 (1996) 526–533.

[21] R. K. Ahluwalia, X. Wang, E. D. Doss R. Kumar, Fuel Cell Systems Analysis, FY 2005 Annual Progress Report, DOE Hydrogen Program, pp. 1014–1018, 2005.